Ionics (2023) 29:2031–2041
https://doi.org/10.1007/s11581-023-04954-8

ORIGINAL PAPER

An electrochemical sensor based on PEI/CS/GN composite–modified glassy carbon electrode for determination of Pb(II)

Yanhong Chen[1] · Sheng Xu[1] · Gang Liu[1] · Wenting Li[1] · Lingli Liu[1] · Zhenxi Wang[1] · Xin Dai[1] · Xinde Jiang[1]

Received: 5 October 2022 / Revised: 23 February 2023 / Accepted: 7 March 2023 / Published online: 15 March 2023

Abstract

A novel electrochemical sensor has been developed in response to sensitive Pb(II) determination with graphene (GN) by ultrasonic dispersed, chitosan (CS) and polyethylene-imine (PEI) composite coated onto the surface of glassy carbon electrode (GCE). The micromorphology, structure, and electrochemical properties of the PEI/CS/GN composite–modified electrode were studied by scanning electron microscopy (SEM), Fourier transform infrared spectroscopy (FTIR), cyclic voltammetry (CV), chronocoulometry (CC), and the differential pulse anodic stripping voltammetry (DPASV). It was discovered that CS/GN electrode provided a significant platform for detection of Pb(II). With the introduction of PEI, the modified electrode demonstrated a good enhancement in voltammetric response because PEI contains large amino groups and has a good response characteristic to heavy metal ions. Moreover, the intensity of volt-ampere response was associated with the weight ratio of PEI, and it displayed a best status when its weight ratio to CS was 30wt%. Under the optimal conditions, there was a great linear correlation ($R^2 = 0.999$) for PEI/CS/GN composite–modified GCE in the Pb(II) concentration range of 0.5 ~ 90 μg/L, and the limit of detection (LOD) was down to 0.01 μg/L based on the signal-to-noise ratio (S/N = 3). The prepared PEI/CS/GN electrode has the advantages of simple preparation, environmental protection, large specific surface area, and rapid electron transport, and which has huge potential application in Pb(II) determination.

Keywords PEI/CS/GN composite · GCE · DPASV · Pb(II) determination

Introduction

The rapid industrialization increased more heavy metal contamination, and all kinds of heavy metals were easy to cause irreversible huge damage to human health [1]. Because heavy metals differ from many organic species, metals cannot turn into harmless compounds as time goes on [2]. As a common heavy metal, lead is so toxic that once it invades into the body, it causes brain cell damage and kills neurons, accompanying symptoms such as nausea, dizziness, and vomiting for people [3]. Due to the increasingly serious problem of water pollution caused by heavy metals, it is urgent need to prepare a detection device with fast, sensitive, and easily portable characteristics.

There are several traditional methods to detect Pb(II) such as atomic absorption spectrometry (AAS) [4–6], mass spectrometry [7, 8], and chromatography [9, 10]. However, these traditional heavy metal detection methods require expensive detection equipment, high power, cumbersome operation steps, and time consumption. Therefore, electrochemical detection methods have been widely studied by virtue of easily portable characteristic, good linear output, and fast response [11]. Currently, the commonly studied methods are square wave anodic stripping voltammetry (SWASV) and differential pulse anodic stripping voltammetry (DPASV). DPASV can effectively reduce the background current generated by the redox reaction of impurities to obtain better detection sensitivity and lower detection limits than SWASV [12]. DPASV is performed by accumulating the measured analyte on the surface of the electrode firstly, and secondly stripping it from the surface of the electrode when scanning potential from negative to positive [13]. Therefore, the

Gang Liu, Wenting Li, Lingli Liu, Xin Dai, and Xinde Jiang contributed equally to this work.

✉ Sheng Xu
xs2953@163.com

✉ Zhenxi Wang
wangzhenxi1978@126.com

[1] College of Sciences, Nanchang Institute of Technology, Nanchang 330099, China

preparation of the working electrode plays a crucial role in the voltammetric analysis of heavy metal ion stripping. And an ideal working electrode should have good reproducibility, sensitivity, selectivity, and anti-interference.

Different modified electrodes have been developed for the determination of heavy metal ions so far, especially the rapidly developing nanotechnology offers more possibilities for electrochemical sensors [14–16]. Nanomaterials with large specific surface area, high electrical conductivity, and good biocompatibility can be used as electrode modified materials and nanocarriers, which greatly amplifies the signal and improves the sensing sensitivity [17, 18]. Graphene with excellent electrical conductivity and two-dimensional planar carriers is usually combined with other materials to improve selectivity of modified electrodes for analytes. The minimal number of functional groups on its surface makes it highly hydrophobic, and it is unable to chelate with metal ions in aqueous solution alone [19]. However, this material is well suitable for combination with bismuth, polymers, or other materials to enhance working electrode performance, which makes graphene a very multifunctional material that can be useful in numerous combinations. Sahoo et al. used RGO/Bi nanocomposites as an electrode material and discovered that RGO/Bi nanocomposites had better properties than single Bi membrane electrodes, providing a better option for heavy metal ion detection. After DPASV detection on Cd(II), Pb(II), Zn(II), and Cu(II) in acetate buffer solution, the LOD for Cd(II), Pb(II), Zn(II), and Cu(II) was obtained as 2.8 μg/L, 0.55 μg/L, 17 μg/L, and 26 μg/L (S/N = 3) at different deposition potentials, respectively [20, 21]. Li et al. fabricated an enhanced electrochemical sensing platform by combing graphene nanosheets dispersed in Nafion solution with in situ bismuth-plated film electrodes for the determination of Pb(II) and Cd(II), the Nafion-graphene composite film electrode had not only a lower detection limit (S/N = 3) around 0.02 μg/L for Pb(II), but also had a good effect on alleviating the interferences due to the synergistic effect of graphene nanosheets and Nafion [22].

CS is another kind of electrode materials used for heavy metal determination due to its unique film-forming property and good adhesion [23]. In addition, CS is a kind of nontoxic polysaccharide which has a large number of $–NH_2$ and –OH groups offering many active chelate sites with heavy metal ions [24]. And it was often combined with other nanomaterials or polymers as a new composite to improve the stability of nanomaterials and electrodes [25]. Deswal et al. reported an improved nanocomplex biosensor based on the covalent synthesis of sarcosine oxidase on nanocomplex CS-graphene nanoribbon and electro-deposition on the surface of Au electrode for the detection of the prostate cancer marker sarcosine. The sensor has a wide linear range of 0.001–100 μM, a minimum detection limit at 0.001 μM, and a high sensitivity [26]. In recent years, polymers are increasingly used in the modification of chemical electrodes due to their abundant functional groups, more active sites, and excellent selectivity. PEI has a high density of amine that it presents a strong complexation to metal ions, and the positively charged PEI can be coupled to the GN surface by both electrostatic self-assembly and covalent encapsulation [27]. Hilal et al. immobilized highly branched polyethyleneimine (PEI) on graphene oxide (GO) to obtain a composite with strong adsorption of arsenic, and its low detection limit was 1.8 ± 0.2 ng/L for As(III) and 1.3 ± 0.08 ng/L for As(V) by chromatographic column procedure, respectively [28]. The results showed that the conductivity and electrochemical stability of the composite were improved by combining PEI with GN.

In this paper, we demonstrated that the combination of PEI/CS/GN composite can provide a low-cost, environmentally friendly and portable composite sensor for electrochemical detection of Pb(II) with high sensitivity and selectivity. The morphology of the composite was determined by scanning electron microscopy (SEM), and the structure was characterized by FTIR. The electrochemical characteristics of the electrode were characterized by CV, CC, and DPASV. The pH, accumulation time, and accumulation potential were systematically optimized to obtain the best experimental conditions in acetate buffer solution. And the applicability of electrodes on Pb(II) detection was verified compared to ICP-OES in actual water sample.

Experimental

Reagents

Graphene (GN, AR, Shenzhen Yuechuang Evolution Technology), chitosan (CS, deacetylation: 80.0–95.0, Sinopharm Chemical Reagent Co., Ltd.), polyethyleneimine (branched PEI, 10,000 M.W., Shanghai Maclean Biochemical Technology Co.), lead nitrate ($Pb(NO_3)_2$, AR (Xilong Science Co., Ltd.), cadmium chloride ($CdCl_2$, AR, Xilong Science Co., Ltd.), calcium chloride hexahydrate ($CaCl_2{\cdot}6H_2O$, AR, Xilong Science Co., Ltd.), cobalt chloride hexahydrate ($CoCl_2{\cdot}6H_2O$, AR, Xilong Science Co., Ltd.), iron chloride ($FeCl_3{\cdot}6H_2O$, AR, Xilong Science Co., Ltd.), nickel acetate tetrahydrate ($NiC_4H_6O_4{\cdot}4H_2O$, AR, Xilong Science Co., Ltd.), zinc acetate dihydrate ($C_4H_6O_4Zn{\cdot}4H_2O$, AR, Xilong Science Co., Ltd.), copper acetate monohydrate ($C_4H_6CuO_4{\cdot}4H_2O$, AR, Xilong Science Co., Ltd.), acetic acid (HAc, AR, Xilong Science Co., Ltd.), sodium acetate trihydrate ($C_2H_3NaO_2{\cdot}3H_2O$, AR, Xilong Science Co., Ltd.), ethanol (CH_3CH_2OH, AR, Xilong Science Co., Ltd.), and alumina polishing powder (Al_2O_3, 0.3 and 0.05 μm, Shanghai Jing Chong Electronic Technology Development Co., Ltd.).

Preparation of the PEI/CS/GN composite

The CS-HAc solution of 5 mg/ml was obtained by dissolving 0.1 g of CS in 20 ml of HAc (0.1 M) and stirring for 2 h. After the chitosan completely dissolved, 0.2g graphene was added into the blended CS-HAc solution and continued stirring for 2 h. After that, PEI with different weight ratio to CS was added and stirred for 6 h (weight ratios of PEI to chitosan: 1 wt%, 5 wt%, 10 wt%, 30 wt%, and 50 wt%). Then, the uniform PEI/CS/GN composite was prepared after ultrasonic dispersed for 20 min using a cell smasher.

Fabrication of the PEI/CS/GN composite–modified GCE

Firstly, the bare electrode was coarse and fine grinded on sandpaper in an "8" pattern, and its surface was polished to be like a mirror with 0.3 and 0.05μm alumina polishing powder, then ultrasonically cleaned with anhydrous ethanol and ultrapure water in turn. The cleaned electrode was placed into a solution of 5 mM potassium ferricyanide ($K[Fe(CN)_6]^{3/4}$) and 0.1 M potassium chloride (KCl) mixed solutions and was scanned by cyclic voltammetry at a rate of 50 mV/s from − 0.34 to 0.60 V to obtain a reversible cyclic voltammetric peak with the peak potential difference of less than 100 mV and the ratio of oxidation to reduction peaks close to 1:1. The scanned glassy carbon electrode was removed and washed with ethanol/water ($V = 1:1$) by ultrasonic. Then, the pretreated glassy carbon electrode was obtained after drying naturally. Subsequently, the prepared PEI/CS/GN composite was applied to the pretreated glassy carbon electrode surface by pipetting 5 μl. Finally, the electrode was dried naturally after 8 h to obtain a PEI/CS/GN composite–modified GCE.

Instrumentation and methods

Cyclic voltammetry (CV), chronocoulometry (CC), and DPASV experiments were detected by an electrochemical workstation (CHI660E, Shanghai Chenhua Instruments Co., Ltd.) with three electrodes including an auxiliary electrode (platinum wire electrode), a reference electrode (Ag/$AgCl_3$), and a working electrode (glassy carbon electrode). Moreover, CV was performed in 0.5 mM $K_3[Fe(CN)_6]$/$K_4[Fe(CN)_6]$ (1:1) and 0.1 M KCl solution. DPASV was performed in 0.1 M acetate buffer solution (pH = 4.75, accumulation time: 120 s, accumulation potential: − 1.0 V, quite time: 5 s). The micromorphology of the modified electrode surface was observed using SEM (TM3030, Hitachi) after ion sputtering gold spray 5 min using gold spraying instrument (LJ-16, Beijing Yulong Times Technology Co., Ltd.). The structure of the modified composite was characterized by using FTIR (NICOLET iS10, ThermoFisher) on a scan rate of 20 min^{-1} from 500 to 4000 cm^{-1} with resolution of 4 cm^{-1}. Xenon light source instrument (PLS-SXE 300, Beijing Porphyry Technology Co.) was employed for sample preparation. ICP-OES (iCAP 7200, ThermoFisher) was used to detect Pb(II) in actual water sample.

Results and discussion

Micromorphological analysis of the PEI/CS/GN composite

Figure 1 shows the SEM images of GN, CS/GN, and PEI/CS/GN composite. By comparing Fig. 1a, b and c, it can be observed that the microscopic morphologies of GN, CS/GN, and 30wt%PEI/CS/GN are distinctly different at × 10,000 magnification. The darker areas in Fig. 1b and c were the dividing line between the districts of composite materials and electrically conductive adhesives. There were the following findings through observing the part inside the dark edge. While graphene shows flaky and crinkled morphology (Fig. 1a), the CS/GN composite exhibits a uniform film (Fig. 1b). After the introduction of PEI, the surface of the films showed the structure of valleys and ridges (Fig. 1c), and the structure was more obvious under × 15,000 magnification (Fig. 1d). It indicated that the PEI with long chains wrapped around graphene facilitated the formation of more folds in graphene, and this fold structure was very beneficial to prevent the inappropriate restacking and aggregation of individual graphene nanosheets. Moreover, it was impossible to distinguish the interface between the PEI and CS phases from Fig. 1b, c, which suggested that PEI phase and CS phase were compatible.

FTIR analysis of the PEI/CS/GN composite

Figure 2 shows the FTIR of GN, CS/GN, and 30wt%PEI/CS/GN composite. The absorption peaks at 3434 cm^{-1}, 2924/2846 cm^{-1}, 1387 cm^{-1}, and 1153 cm^{-1} are the characteristic absorption peaks of –OH/–NH_2 [29], –CH_2– [30], –CN– [31], and –C–O– [32], respectively. The stretching vibration peaks at 2924 and 2846 cm^{-1} are due to –CH_2– in aliphatic and aromatic groups, PEI is a long-chain polymer of large molecules containing a large amount of –CH_2– and –NH_2, so PEI/CS/GN composite appears strong vibrational peaks at 2924, 2846, and 3434 cm^{-1} in the FTIR curves compared with CS/GN composite at the same wavenumbers. The –C–O– stretching vibrational peak at 1153 cm^{-1} is attributed to the CS/GN composite. These all above analyses indicate that the PEI/CS/GN composite is prepared successfully.

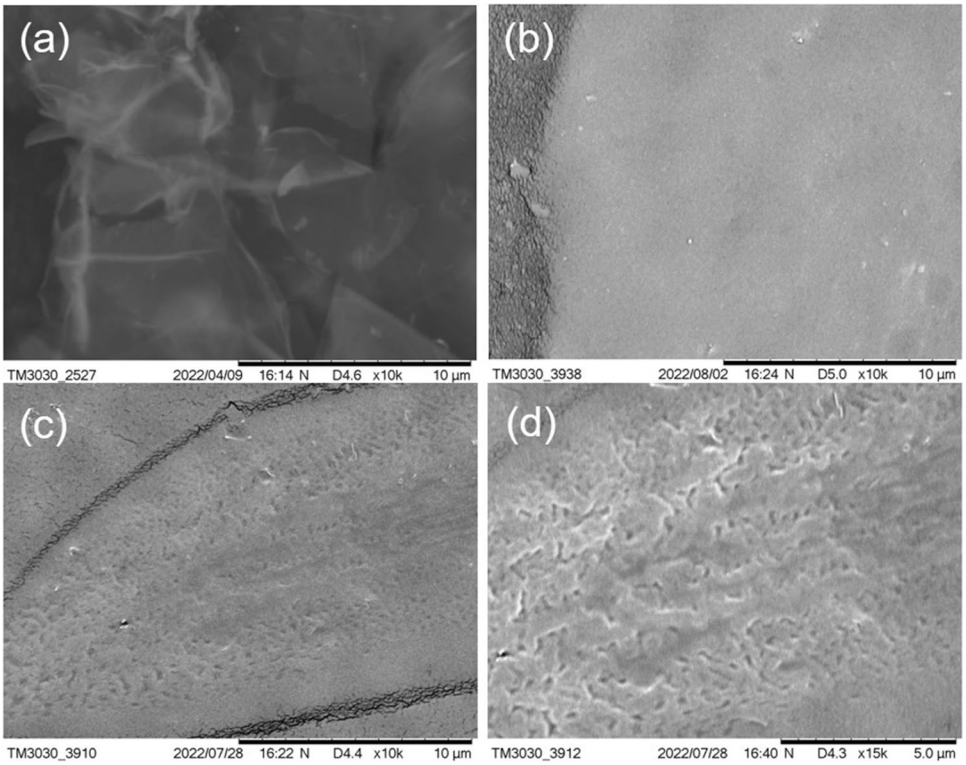

Fig. 1 SEM images: **a** GN (×10,000); **b** CS/GN composite (×10,000); **c** 30wt%PEI/CS/GN composite (×10,000); **d** 30wt%PEI/CS/GN composite (×15,000)

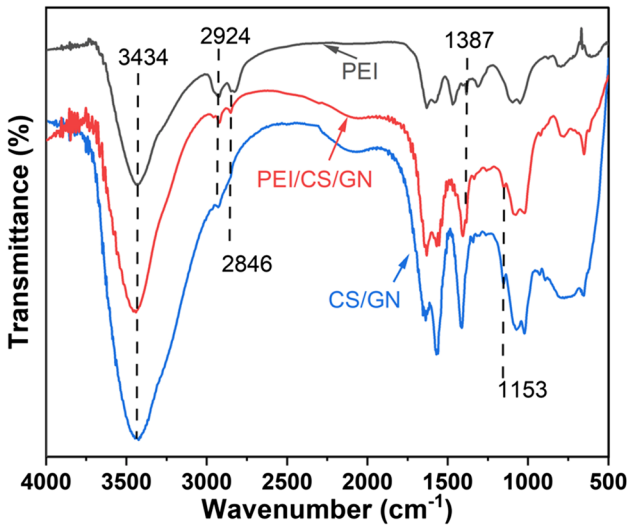

Fig. 2 Fourier transform infrared spectra of GN, CS/GN composite, and 30wt%PEI/CS/GN composite

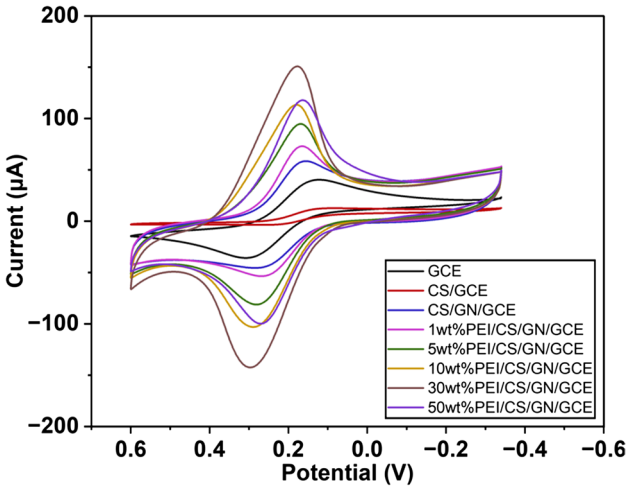

Fig. 3 Cyclic voltammograms plots of GCE, CS, CS/GN composite, and PEI/CS/GN composite electrodes

CV analysis

Figure 3 shows the electrochemical characterization of the different modified glassy carbon electrode in 0.5 mM $K_3[Fe(CN)_6]/K_4[Fe(CN)_6]$ and 0.1 M KCl solutions. The higher redox peak current in the CV cyclic voltammogram indicates the faster electron transfer rate between the electrode and $[Fe(CN)_6]^{3-/4-}$, and the higher redox peak intensity and the lower peak voltage difference (ΔE_p) indicates the better reversibility of the electrochemical reaction [33]. By comparing the cyclic voltammograms of the GCE, CS electrode, CS/GN modified electrode, and PEI/CS/GN composite–modified electrode, it can be observed that the introduction of graphene increases the redox peak current of the electrode, which is further increased by the introduction of PEI. For CS electrode (the red curve) showed a weak redox peak and increasing ΔE_p value (180 mV). That is

attributed to the orthogonal crystal structure of CS in which there are very strong hydrogen bonding interactions, thus limiting the ion transport properties and resulting in very a weak ionic conductivity to obstruct the electron transfer between electrodes and $[Fe(CN)_6]^{3-/4-}$ [34]. The redox peak current of the PEI/CS/GN composite–modified electrode gradually increased with the increase of PEI content, which reaches to the maximum with 150 μA; meanwhile, the ΔE_p value decreased from 188 (bare electrode) to 118 mV when the weight ratio of PEI to CS is 30%. However, the CV plot of 50wt%PEI/CS/GN electrode descended to near that of 10wt%PEI/CS/GN electrode. Thus, we presumed that, on one hand, in the composite matrix, the increase of PEI content will inevitably lead to the decrease of GN content. On the other hand, excessive PEI component was disadvantaged for the electron transfer due to its insulativity, even though high content of PEI was better for the enrichment of Pb(II) in aqueous solution. The data analysis above indicates that the PEI/CS/GN composite has the advantages of good electrochemical reactivity, fast electron transfer rate, and good reversibility of electrochemical reactions.

Electrochemical effective surface area analysis

The chronocoulometric approach is an electrochemical characterization method that can be used to study the electrochemical effective surface area of an electrode, which can be calculated by Anson's equation (Eq. 1) [35] and the slope of Q versus $t^{1/2}$ (Fig. 4b) which was original from Q-t curves in Fig. 4a:

$$Q(t) = \frac{2nAFcD^{1/2}t^{1/2}}{\pi^{1/2}} + Q_{dl} + Q_{ads} \quad (1)$$

The n, A, F, c, D corresponds to the number of electron transfers, effective surface area, Faraday constant, the concentration of reactants, and the diffusion coefficient of electrochemical activity in the solution system, respectively. And Q_{dl} represents the charging charge of the bilayer, and Q_{ads} is Faraday charge in the equation. In 5 mM $K_3[Fe(CN)_6]$ and 0.1 M KCl solution, $n = 1$, $D = 6.67 \times 10^6$ cm^2/s [36]. When the Q-$t^{1/2}$ curve passes the coordinate origin, Q_{dl} and Q_{ads} are zero. Therefore, the A of GCE, pure CS, and CS/GN composite electrodes were 0.117 cm^2, 0.074 cm^2, and 1.362 cm^2, respectively. The A of pure CS electrode was reduced because of dense film structure and poor electrical conductivity. With introduction of GN, the A of prepared electrodes had a dramatic increase due to the excellent electrical conductivity and high electronic transfer rate of GN. After the introduction of different weight ratio PEI, the A of 1 to 50wt%PEI/CS/GN electrodes were 1.529 cm^2, 1.630 cm^2, 1.701 cm^2, 1.921 cm^2, and 1.808 cm^2. There was a very perfect regularity about increase on A of the electrode with increase on PEI weight ratio until it reached the maximum value at the weight ratio of 30% to CS, and the A of the 30wt%PEI/CS/GN composite electrode was 16-fold ones of bare GCE. Above all, it indicated that PEI's long-chain advantage and a large number of reactive groups promoted high active site surface of CS/GN electrodes. However, the A of 50wt%PEI/CS/GN electrodes had slightly reduced; the main reason was that the excessive PEI content led to a decrease in the percentage of GN per unit volume which caused a decrease in the reactive sites of prepared electrode surface. The calculation results showed that the introduction of GN could increase the A of the electrode, while the addition of PEI further increased the electrochemical effective surface area of the modified electrode. It proved that the PEI/CS/GN composite–modified GCE provided a sensitive conductivity platform for the detection of heavy metal ions.

DPASV analysis of the PEI/CS/GN composite–modified GCE

Figure 5 shows the response curves of bare GCE against CS, CS/GN and 1 ~ 50wt% PEI/CS/GN composite–modified GCE in 0.1 M acetate buffer solution (pH = 4.75) for the detection of 50 μg/L Pb(II). The magnitude of the voltammetric current obtained using the DPASV represents

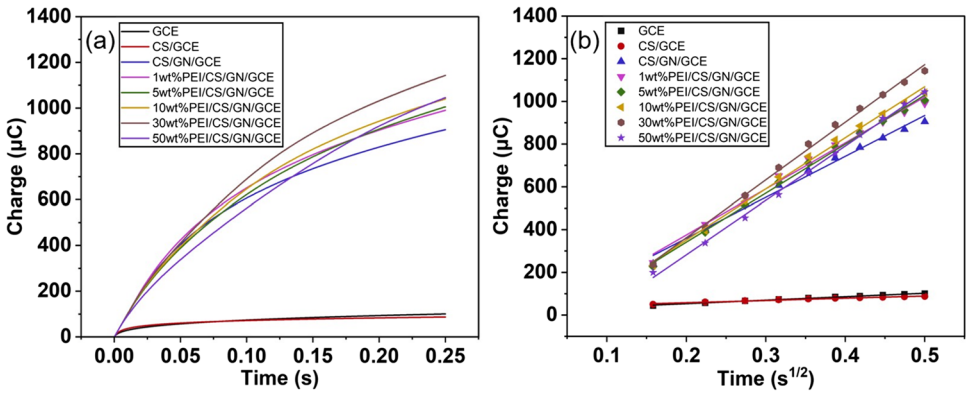

Fig. 4 **a** Plot of Q-t curves and **b** plot of Q-$t^{1/2}$ curves of bare GCE, CS, CS/GN, and PEI/CS/GN composite electrodes

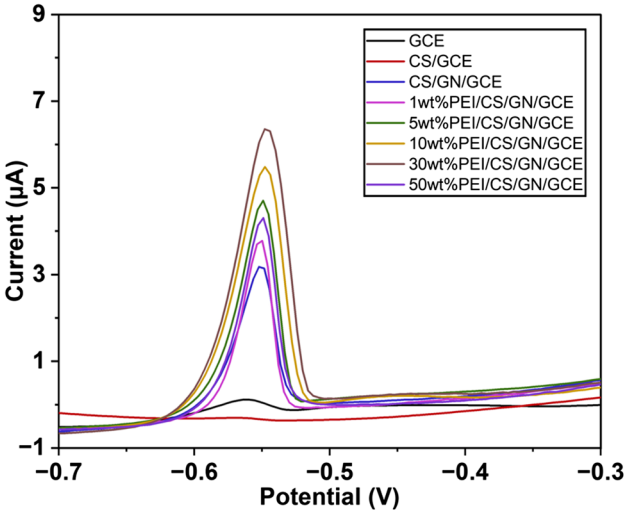

Fig. 5 DPASV curves of bare GCE, CS, CS/GN composite and PEI/CS/GN composite electrodes

the amount of Pb(II) concentration, so the higher intensity of the voltammetric response and the higher peak value indicate that the electrode has better selectivity and higher sensitivity for Pb(II). The figure shows that the stripping potential of Pb(II) is about − 0.55 V. A tiny peak appeared for the bare GCE, which is also confirmed by the previous research [37–39]. And the single CS film electrode had a weaker stripping peak current on its surface than GCE. The worse DPASV response maybe resulted by the poor electrical conductivity of CS. Although the pure CS film electrode has many active sites on its surface, the poor conductivity of CS severely hinders the electron transfer between Pb(II) and the modified electrode. After the introduction of graphene, the current peak of the CS/GN electrode was obviously increased. Compared to CS/GN electrode, the DPASV response current of PEI/CS/GN composite electrode was better and gradually increased with the increase of PEI content, reaching the maximum peak at 30wt% and then decreasing with the increase over 30wt%, which fitted well with the previous analysis of CV and CC. Moreover, the magnitude of the DPASV response current for PEI/CS/GN composite electrode is significantly larger than that for CS/GN electrode. This is mainly attributed to the larger specific surface area of PEI/CS/GN composite material, which facilitates the rapid transfer of electrons and the enhancement of heavy metal ion signals. In addition, the DPASV response also demonstrates the accuracy of the above cyclic voltammetry electrochemical effective surface area analysis, and this result indicates that the PEI/CS/GN composite–modified electrode is more sensitive than the bare GCE, CS, and CS/GN composite–modified electrodes for Pb(II) with better detection performance. Moreover, the reactions can be described by the following: $R\text{-}NH_2 + H^+ \rightarrow R\text{-}NH_3^+$ and $R\text{-}NH_3^+ + Pb^{2+} \rightarrow R\text{-}NH_2Pb^{2+} + H^+$. The amine group is protonated in acidic environment to form cationic $–NH_3^+$, then the ammonium group coordinates with Pb(II) to form a stable chelate.

Optimization of experimental conditions

In order to obtain greater sensitivity and accuracy for the 30wt%PEI/CS/GN composite–modified GCE, it is necessary to optimize the parameters such as pH of acetate buffer solution, accumulation time, and accumulation potential involved in the experimental conditions.

Figure 6a shows the effect of acetate buffer solution pH on the differential pulse anodic stripping voltammetric response current on 30wt%PEI/CS/GN composite–modified GCE. It can be seen from the line graph of pH effect that the peak current increases when the pH of acetate buffer solution increases from 3 to 4.75, and then, the peak current gradually shows a decreasing trend from 4.75 to 6. The reason for this result was that the amino protonation ($–NH_3^+$) level on CS and PEI was influenced by pH value. The amino protonation was dramatic when the pH of the buffer solution was low (pH = 3 ~ 4.75), which was easy to cause electrostatic repulsion reaction with positively charged heavy metal ions and blocked the attraction of Pb(II) to the electrode

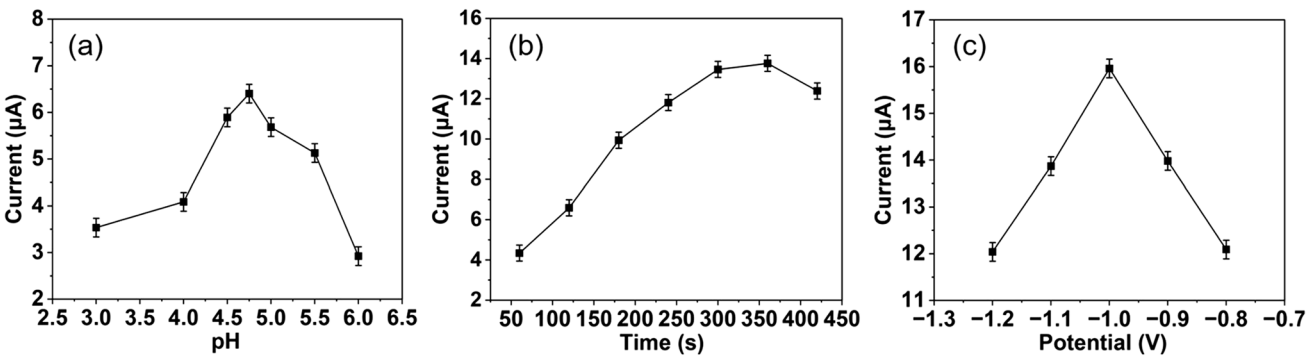

Fig. 6 Effect of **a** pH of acetate buffer solution, **b** accumulation time, **c** accumulation potential of 30wt%PEI/CS/GN/GCE

surface. When the pH gradually increased, the level of amino protonation decreased and the electrostatic attraction of electrode to Pb(II) increased, and led to increase of peak current to Pb(II). However, the hydrolysis of Pb(II) will play an important role when the pH > 4.75 and led to a decrease of stripping peak current to Pb(II) gradually. Therefore, the pH of the acetate buffer solution was set at 4.75 for the next experiments. As the accumulation time gradually increased from 60 to 360 s, the DPASV response gradually increased and stabilized at 360 s as shown in Fig. 6b, so 360 s was the optimal accumulation time under this experimental condition. The effect of accumulation potential on the peak current of DPASV was investigated by accumulation of lead ions in acetate buffer solution containing 50 µg/L Pb(II) at pH 4.75 for 360 s. From − 1.2 to − 1.0 V, the peak current of Pb(II) dissolution gradually increased, and from − 1.0 to − 0.8 V, the peak current of Pb(II) dissolution gradually decreased (shown in Fig. 6c), so − 1.0 V was selected as the optimal enrichment potential.

Performance analysis of the 30wt%PEI/CS/GN composite–modified GCE

Figure 7a shows the peak voltage of Pb(II) on 30wt%PEI/CS/GN composite–modified GCE near − 0.54 V. The peak current increases with increasing Pb(II) ion concentration. Under optimal conditions, Pb(II) showed a linear correlation in the concentration interval of 0.5 to 90 µg/L (in Fig. 7b), and the linear regression equation was $i_p\ (\mu A) = 0.0748 \times C\ (\mu g/L) - 0.0509$, with a correlation coefficient of 0.999. Based on the signal-to-noise ratio of 3 (S/N = 3), the limit of detection (LOD) of 30wt%PEI/CS/GN composite–modified electrode was 0.01 µg/L after 360 s of Pb(II) deposition, which was lower than the WHO standard of 10 µg/L. For the detection of Pb(II), this electrode outperformed other modified materials reported in the relevant literature, such as multi-walled carbon nanotubes [18], bismuth film [21], Nafion-graphene composite film [22], RGO oxidized-chitosan/polymerized-L-lysine nanocomposite [24], polyvinyl alcohol/chitosan-thermally reduced graphene composite [25], as shown in Table 1.

Anti-interference, repeatability, and reproducibility experiments

The DPASV detection of a particular heavy metal ion is susceptible to interference from other heavy metal ions, and the stable output of the peak current of the dissolved lead ion may be affected when other ions are present in the acetate buffer solution. Especially, cadmium, which coexists with lead in common real samples, is considered as a very potential interference for electrochemical detection of lead. In this experiment, the effect of Cd(II) on the DPASV curve of Pb(II) at this modified electrode was investigated. Keeping the concentration of Cd(II) constant and increasing the concentration of Pb(II), the peak current corresponding to Cd(II) was hardly changed (shown in Fig. 8). The linearity of Pb(II) was obtained in the

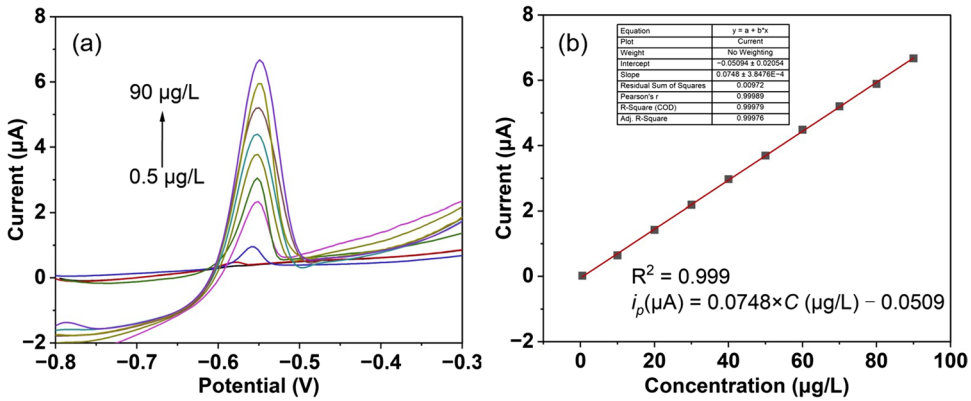

Fig. 7 **a** DPASV curves of 30wt%PEI/CS/GN composite–modified GCE in 0.5, 10, 20, 30, 40, 50, 60, 70, 80, and 90 µg/L Pb(II); **b** calibration curve for 0.5 ~ 90 µg/L Pb(II) detection

Table 1 Comparison of the electrochemical analysis of Pb(II) detection for PEI/CS/GN/GCE and others

Electrodes	Methods	Linear range (µg/L)	LOD (µg/L)	References
Polyfurfural film/MWCNTs/GCE	DPASV	0.1–15	0.01	[18]
Carbon dots modified bismuth film/GCE	DPV	50–500	2.3	[21]
Nafion-graphene composite film/GCE	DPASV	0.5–50	0.02	[22]
RGO oxide-chitosan/poly-L-lysine/GCE	DPASV	0.05–10	0.02	[24]
PVA/chitosan-TRG/GCE	SWASV	1–50	0.05	[25]
PEI/CS/GN/GCE	DPASV	0.5–90	0.01	This work

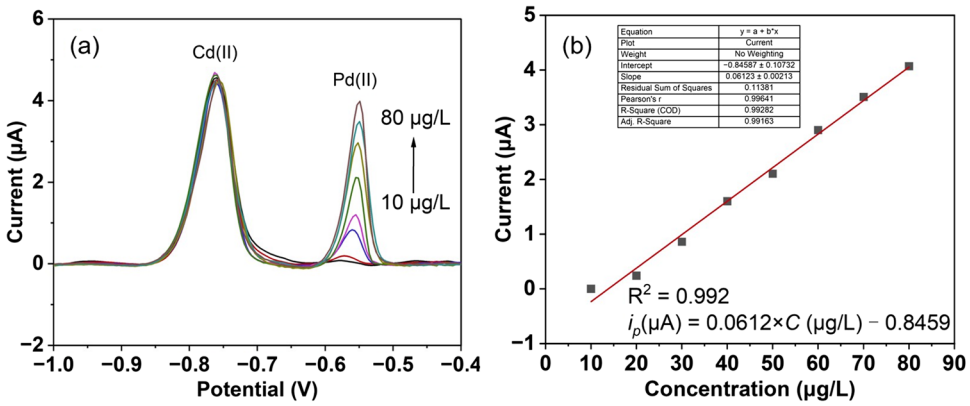

Fig. 8 **a** DPASV curves of 30wt%PEI/CS/GN composite–modified GCE in 10, 20, 30, 40, 50, 60, 70, and 80 μg/L Pb(II) coexisting with 20 μg/L Cd(II); **b** calibration curve for 10 ~ 80 μg/L Pb(II) detection

concentration interval from 10 to 80 μg/L with the linear equation $i_p\,(\mu A) = 0.0612 \times C\,(\mu g/L) - 0.8459$, and the correlation coefficient was 0.992. And the sensitivity obtained was close to that when only one heavy ion was present (0.0748 μA·L/μg versus 0.0612 μA·L/μg). This indicates that the co-presence of Pb(II) with 20 μg/L of Cd(II) does not interfere with the Pb(II) detection.

In order to demonstrate that the electrode is also highly resistant to other common external ions, the 30wt%PEI/CS/GN composite–modified GCE was placed in 0.1 M acetate buffer solution containing 50 μg/L of Pb(II) and 10 times concentration of interfering ions separately such as Ca^{2+}, Co^{2+}, Fe^{3+}, Ni^{2+}, Zn^{2+}, Cu^{2+}, Cl^{-}, and NO_3^{-}. After six DPASV scans, the results showed that the relative standard deviation (RSD) of the peak currents of Pb(II) response for 50 μg/L in the coexisting other ionic acetate solutions were less than 5%, and exhibited in Fig. 9. As for Cu^{2+}, the two times concentration of lead ions would interfere with the detection process seriously, only a weak stripping peak appeared around − 0.54 V. This may be caused by the formation of a copper-lead alloy during the deposition process which blocked the following lead ion deposition. Therefore, ferricyanide should be used to resist the interference of Cu^{2+}. According to the above analysis, the other ions basically did not interfere with the detection of Pb(II) except Cu(II).

The repeatability of the 30wt%PEI/CS/GN composite–modified GCE was studied with five independent measurements under optimized conditions in the solution containing 40 μg/L, 50 μg/L, and 60 μg/L Pb(II). According to the results, the RSD was calculated to be 4.5%, 3.2%, and 1.7%, respectively (shown in Fig. 10a, b, c). The electrode was reserved for 3 weeks, and its relative standard deviation of the peak current was 3.4% after five DPASV scanning in acetate solution with 50 μg/L Pb(II) (shown in Fig. 10d), and the current strength still maintained at 94% of the original level.

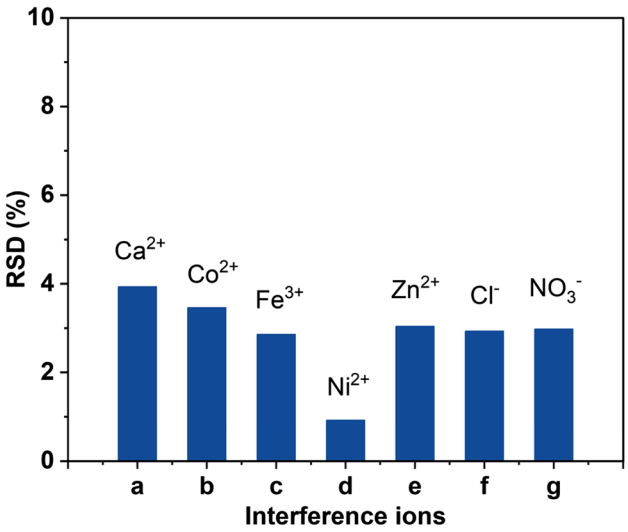

Fig. 9 Anti-interference experiments for Pb(II) under interfering ions of 10 times lead concentration (**a** Ca^{2+}, **b** Co^{2+}, **c** Fe^{3+}, **d** Ni^{2+}, **e** Zn^{2+}, **f** Cl^{-}, **g** NO_3^{-})

Pb(II) detection in actual water sample

The accuracy and availability of the PEI/CS/GN electrode can be demonstrated by applying it to detect Pb(II) in actual water samples compared with ICP-OES. Five water samples were collected from tap water, two local rivers, and two local lakes, respectively. All collected water samples are treated using water bath digestion method [12]. Organic and reducing substances were dissolved by 65% nitric acid (HNO_3) and 30% hydrogen peroxide (H_2O_2) before filtering through a 0.2μm membrane and Xenon light source instrument lighted for 2 h to decompose the organic lead into inorganic form. Then, 1 ml of each water simple was added into acetate buffer solution of pH = 4.75. Table 2 shows the Pb(II) detection results in five different actual water samples by using DPASV and ICP-OES. After three parallel Pb(II) detection under optimal conditions, the results were generally consistent. Therefore, the PEI/CS/GN electrode

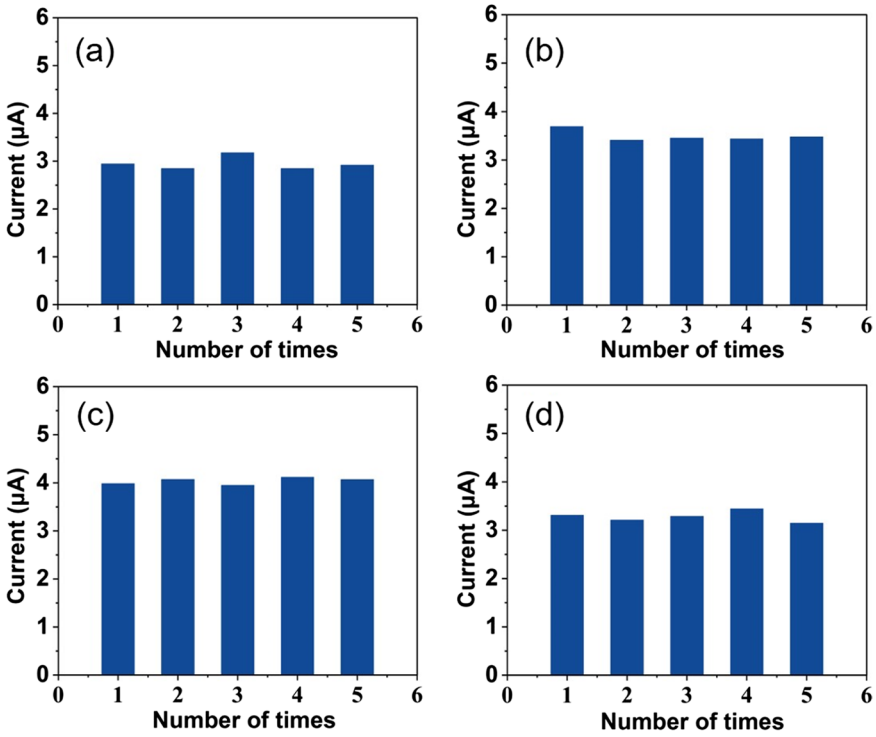

Fig. 10 Repeatability experiments with different Pb(II) concentration: **a** 40 μg/L Pb(II), **b** 50 μg/L Pb(II), **c** 60 μg/L Pb(II); **d** reproducibility experiments with 50 μg/L Pb(II)

Table 2 Pb(II) detection in actual water samples by the PEI/CS/GN electrode and ICP-OES

Number	Actual water simples	PEI/CS/GN/GCE (μg/L)	ICP-OES (μg/L)
1	Tap water	< LOD	< LOD
2	River 1	10.05 ± 3	11.21
3	River 2	17.23 ± 3	18.35
4	Lake 1	29.18 ± 2	27.29
5	Lake 2	5.11 ± 2	3.65

has an excellent application for Pb(II) detection in actual water sample.

Conclusions

In summary, we successfully fabricated an electrochemical sensor based on PEI/CS/GN composite as a sensitive layer for determination of Pb(II). PEI/CS/GN composite was prepared by ultrasonic exfoliation and characterized by SEM, FTIR, and CHI660E electrochemical workstation. The combination of CS/GN and PEI can provide a sensitive electrochemical sensing platform to target heavy metal detection with a larger active surface area and good electrical conductivity. The electrochemical behavior of the prepared sensors for Pb(II) was analyzed by DPASV. When introducing 30wt% PEI, the electrode displayed the best sensitivity to Pb(II) determination. After condition optimization, the best conditions of DPASV experiments were pH = 4.75, 360 s accumulation time, and − 1.0 V accumulation potential for the 30wt%PEI/CS/GN composite electrode in 0.1 M acetate buffer solution. The Pb(II) detected by electrochemical methods had a wide linear range: 0.5 ~ 90 μg/L with a high linear correlation coefficient ($R^2 = 0.999$), and the LOD was 0.01 μg/L (S/N = 3). In this study, the prepared electrode had a good anti-interference with Ca^{2+}, Co^{2+}, Fe^{3+}, Ni^{2+}, Zn^{2+}, Cl^-, and NO_3^-. The RSDs of the prepared electrode were all less than 5% in the reproducibility experiments. The results above showed a good sensitivity, good interference immunity, and reproducibility. Thus, this work provides a novel and effective analytical strategy for the highly sensitive determination of heavy metal ions in the future.

Author contribution Sheng Xu designed the experiments; Yanhong Chen completed the experiments and wrote this manuscript; Gang Liu and Wenting Li analyzed the experiment data. All the authors read and revised the final manuscript.

Funding This work was supported by the Jiangxi Provincial Department of Education Natural Science Foundation of China (GJJ190983); the Jiangxi Provincial Natural Science Foundation of China (20224BAB203024, 20202BAB213010); Jiangxi Provincial Key Research and Development Foundation (20202BBFL63022); Jiangxi Provincial Science and technology Major Project (20203ABC28W016); Sub-project of Camphor tree Research of Jiangxi Forestry Bureau (20200504).

Data availability The authors confirm that the data and materials supporting the findings of this study are available within the article.

Declarations

Ethics approval Not applicable.

Consent to participate Not applicable.

Consent for publication Not applicable.

Competing interests The authors declare no competing interests.

References

1. Zhou Y, Yi ZH, Song D, Wang HL, Zhao SP, Long F, Zhu A (2022) Development of a two-in-one integrated bioassay for simultaneous and rapid on-site detection of Pb^{2+} and Hg^{2+} in water. Anal Chim Acta 11(94):339397–339405
2. Humberto APL, Fernando RA, Victor HPG, Sergio OMC, Roberto CGV (2022) Nanomaterials for electrochemical detection of pollutants in water: a review. Electroanalysis 43(1):249–262
3. Nodehi M, Baghayeri M, Kaffash A (2022) Application of BiNPs/MWCNTs-PDA/GC sensor to measurement of Tl (1) and Pb (II) using stripping voltammetry. Chemosphere 301:134701
4. Agustina M, Mulyono TW (2021) Assessment of heavy metal lead (Pb) contents in canned crab products by atomic absorption spectrophotometry (AAS). IOP Conf Ser Earth Environ Sci 679(1):012012–012016
5. Ayutthaya PIN, Yeerum C, Kesonkan K, Kiwfo K, Grudpan K, Teshima N, Mu RH, Vongboot M (2021) Determination of lead employing simple flow injection AAS with monolithic alginate-polyurethane composite packed in-valve column. Molecules 26(15):4397–4405
6. Joelem CM, Wellington CC, Elane SBM, Rennan OA, Daniele CMBS (2020) Sequential determination of Cd Co, Cu, Fe, Mg, Mn, Ni, Pb, and Zn in powdered refreshments by FS-F AAS after a simple sample treatment. Food Anal Methods 13(1):212–221
7. Wang YP, Lou SC, Liu X, Zhao LF (2020) Detection of trace metal ions in high-purity boric acid by online two-dimensional valve switching coupled with ion chromatography-inductively coupled plasma mass spectrometry. Microchem J 155:104661–104668
8. Zhou LH, Jin YJ, Ma LF, Huang WH, Li M, Wu Y, Cao XL (2022) Multi-isotope calibration for determination of nickel, molybdenum, barium and lead in soil samples by inductively coupled plasma mass spectrometry. Spectrosc Lett 55(4):278–283
9. Qasim U (2020) Separation and analysis of heavy metal ions by thin-layer chromate-graphy (TLC)—a mini-review (2000–2019). JPC—J Planar Chromatogr— Modern TLC 33(4):1–12
10. Wang J, Wang QL, Luo Y, Gao T, Zhao YW, Pei RJ (2019) In vitro selection of ssDNA aptamers that can specifically recognize and differentiate riboflavin and its derivative FAD. Talanta 204:424–430
11. Baghayeri M, Alinezhad H, Fayazi M, Tarahomi M, Ghanei-Motlagh R, Maleki B (2019) A novel electrochemical sensor based on a glassy carbon electrode modified with dendrimer functionalized magnetic graphene oxide for simultaneous determination of trace Pb(II) and Cd(II). Electrochim Acta 312:80–88
12. Somkid M, Chooto P (2019) Determination of lead(II) and cadmium(II) in water lily stems using a bismuth film electrode. J Electrochem Sci Eng 9(3):153–164
13. Wang TT, Yue W (2017) Carbon nanotubes heavy metal detection with stripping voltammetry: a review paper. Electroanalysis 29(10):2178–2189
14. Maleki B, Baghayeri M, Ghanei-Motlagh M, Zonoz FM, Amiri A, Hajizadeh F, Hosseinifar AR, Esmaeilnezhad E (2019) Polyamidoamine dendrimer functionalized iron oxide nanoparticles for simultaneous electrochemical detection of Pb^{2+} and Cd^{2+} ions in environmental waters. Measurement 140:81–88
15. Deshmukh MA, Mahendra DS, Almira R, Arunas R (2018) Composites based on conducting polymers and carbon nanomaterials for heavy metal lon sensing (review). Crit Rev Anal Chem 48(4):293–304
16. Hina L, Muhammad I, Shoomaila L, Nazim H, Muhammad B (2022) Multifunctional nanomaterials and nanocomposites for sensing and monitoring of environmentally hazardous heavy metal contaminants. Environ Res 214(P1):113795–113811
17. Baghayeri M, Amiri A, Karimabadi F, Masi SD, Maleki B, Adibian F, Pourali AR, Malitesta C (2021) Magnetic MWCNTs-dendrimer: a potential modifier for electrochemical evaluation of As (III) ions in real water samples. J Electroanal Chem 888:115059
18. Huang JZ, Bai SL, Yue GQ, Chen WX, Wang LS (2017) Coordination matrix/signal amplifier strategy for simultaneous electrochemical determination of cadmium(II), lead(II), copper(II), and mercury(II) ions based on polyfurfural film/multi-walled carbon nanotube modified electrode. RSC Adv 7(45):28556–28563
19. Huang H, Chen T, Liu XY, Ma HY (2014) Ultrasensitive and simultaneous detection of heavy metal ions based on three-dimensional graphene-carbon nanotubes hybrid electrode materials. Anal Chim Acta 852:45–54
20. Sahoo PK, Bharati P, Sahoo S, Satpiti AK, Li D, Bahadur D (2013) In situ synthesis and properties of reduced graphene oxide/Bi nanocomposites: as an electroactive material for analysis of heavy metals. Biosens Bioelectron 43:293–296
21. Zhang H, Cui J, Zeng YX, Zhang Y, Pei YS (2022) Direct electrodeposition of carbon dots modifying bismuth film electrode for sensitive detection of Cd^{2+} and Pb^{2+}. J Electrochem Soc 169(1):017501–017510
22. Li J, Guo SJ, Zhai YM, Wang EK (2009) High-sensitivity determination of lead and cadmium based on the Nafion-graphene composite film. Anal Chim Acta 649(2):196–201
23. Kannaiyan P, Dhamodaran MS, Panneerselvam RS, Jayaprakash K, Subash CB (2019) Voltammetric determination of caffeic acid byusing aglassy carbon electrode modified with achitosan-protected nanohybrid composed of carbon black and reduced graphene oxide. Mikrochim Acta 186(2):54
24. Guo Z, Li DD, Luo XK, Li YH, Zhao QN, Li MM, Zhao YT, Sun TS, Ma C (2017) Simultaneous determination of trace Cd(II), Pb(II) and Cu(II) by differential pulse anodic stripping voltammetry using a reduced graphene oxide-chitosan/poly-L-lysine nanocomposite modified glassy carbon electrode. J Colloid Interface Sci 490:11–22
25. Linh DN, Tin CDD, Tien MH, Vu NPN, Hiep HD, Dung MTD, Chien MD (2021) An electrochemical sensor based on polyvinyl alcohol/chitosan-thermally reduced graphene composite modified glassy carbon electrode for sensitive voltammetric detection of lead. Sens Actuators B Chem 345:130443
26. Deswal R, Vinay N, Kumar P, Verma V, Dang AS, Pundir CS (2022) An improved amperometric sarcosine biosensor based on graphene nanoribbon/chitosan nanocomposite for detection of prostate cancer. Sensors Int 3:100174–100181
27. Weng Y, Bo J, Yang K, Sui Z, Zhang L, Zhang Y (2015) Polyethyleneimine-modified graphene oxide nanocomposites for effective protein functionalization. Nanoscale 7:14284–14291
28. Halil A, Khalid U, Syed GA, Priyanka S, Sheikh SI, Haris MK (2018) Preconcentration and speciation of arsenic by using a graphene oxide nanoconstruct functionalized with a hyperbranched polyethyleneimine. Microchim Acta 185(6):290–296

29. Chirag BG, Serena G, Stefano M, Maria SP, Nicola S, Enrico M (2019) Depolymerization of waste poly (methyl methacrylate) scraps and purification of depolymerized products. J Environ Manage 231:1012–1020
30. Leila RR, Arash M, Babak FG, Mohammad I, Mehri M, Bahareh N (2014) Removal of Ni^{2+} and Cd^{2+} ions from aqueous solutions using electrospun PVA/zeolite nanofibrous adsorbent. Chem Eng J 256:119–127
31. Cao N, Lin ZY, Sun RY, Chen LY, Pan JH, Jiang ZH (2021) Repairing of graphene oxide membranes based on SPEEK substrate for organic solvents nanofiltration through PEI needle thread method. Carbon 185:39–47
32. Lee DW, De LSVL, Seo JW, Leon FL, Bustamante DA, Cole JM, Barnes CHW (2010) The structure of graphite oxide: investigation of its surface chemical groups. J Phys Chem B 114(17):5723–5728
33. Yao JX, Zhang K, Wang W, Zuo XQ, Yang Q, Wu MG, Li G (2018) Great enhancement of electrochemical cyclic voltammetry stabilization of Fe_3O_4 microspheres by introducing 3DRGO. Electrochim Acta 279:168–176
34. Wu M, Zhang X, Zhao Y, Yang CP, Jing SS, Wu QS, Alexandra B, Jeffrey TM, Nicole JL, Wu T, Sahana B, Mounesha NG, Zhang YG, Qi Y, Steven GG, Robert MB, Yan YS, Hu LB (2022) A high-performance hydroxide exchange membrane enabled by $Cu2^{+}$-crosslinked chitosan. Nat Nanotechnol 17(6):629–636
35. Justin GJ, Rahmat W, Liu JQ, Yang WR, Dusan L, Shannon O, Mearns Freya J, Shapter Joe G, Brynn HD (2003) Protein electrochemistry using aligned carbon nanotube arrays. J Am Chem Soc 125(30):9006–9007
36. Lee S, Oh J, Kim D, Piao YZ (2016) A sensitive electrochemical sensor using an iron oxide/graphene composite for the simultaneous detection of heavy metal ions. Talanta 160:528–536
37. Zhou WS, Li CH, Sun C, Yang XD (2015) Simultaneously determination of trace Cd^{2+} and Pb^{2+} based on L-cysteine/graphene modified glassy carbon electrode. Food Chem 192:351–357
38. Lee S, Park SK, Eunjin C, Piao YZ (2016) Voltammetric determination of trace heavy metals using an electrochemically deposited graphene/bismuth nanocomposite film-modified glassy carbon electrode. Electroanal Chem 766:120–127
39. Jaime P, Rodrigo S, Diego T, Soledad B, Paulina SR (2019) Electroanalytical determination of Cd(II) and Pb(II) in bivalve mollusks using electrochemically reduced graphene oxide-based electrode. Electroanalysis 31(11):2199